ACS APPLIED MATERIALS & INTERFACES

Research Article

www.acsami.org

Polystyrene Templated Porous Titania Wells for Quantum Dot Heterojunction Solar Cells

Cheng Cheng,[†] Michael M. Lee,[‡] Nakita K. Noel,[‡] Gareth M. Hughes,[†] James M. Ball,[‡] Hazel E. Assender,[†] Henry J. Snaith,*[,‡] and Andrew A. R. Watt*[,†]

[†]Department of Materials, University of Oxford, Parks Road, Oxford OX1 3PH, United Kingdom

[‡]Clarendon Laboratory, Department of Physics, University of Oxford, Parks Road, Oxford OX1 3PU, United Kingdom

Supporting Information

ABSTRACT: Polystyrene spheres are used to template TiO_2 with a single layer of 300 nm wells which are infilled with PbS quantum dots to form a heterojunction solar cell. The porous well device has an efficiency of 5.7% while the simple planar junction is limited to 3.2%. Using a combination of optical absorption and photocurrent transient decay measurement we determined that the performance enhancement comes from a combination of enhanced optical absorption and increased carrier lifetime.

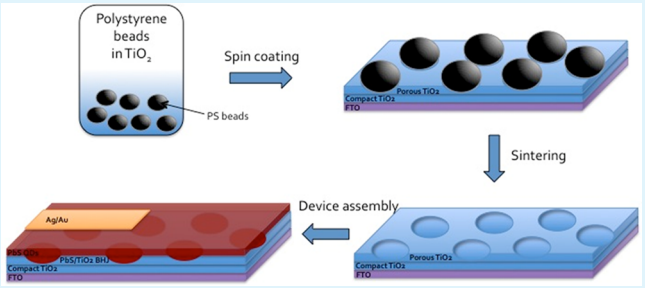

KEYWORDS: *PbS, colloidal quantum dot, photovoltaic, polystyrene template, heterojunction, porous TiO_2*

INTRODUCTION

Improvements in the power conversion efficiency of quantum dot (QD) solar cells is currently propelled by both improving the electronic properties of materials[1−5] and designing novel device architectures.[6−13] Some of the best performing QD solar cells reported to date have utilized an interpenetrated donor−acceptor bulk heterojunction structure which simultaneously gives good light absorption and charge extraction.[6,13] In this paper we use polystyrene beads to template a titanium dioxide electrode to create a single layer of 300 nm wells which can be easily filled with QDs to maximize the donor−acceptor interface and enhance device efficiency through improved absorption of light and charge collection pathways.

In a thick planar junction device, a charge extraction "dead zone" exists close to the top electrode where excited carriers are not extracted as photocurrent. This is due to the film thickness exceeding the depletion region and diffusion length of minority carriers. To overcome this 3-D bulk heterojunction is used to extend the junction interface through the absorber layer thus allowing more photons to be harvested.[6,7] The bulk heterojunction morphology is engineered such that the dimensions of the two phases are at the same scale as the exciton diffusion length in the case of an excitonic junction[14,15] or the width of the depletion region in the case of a p−n junction.[6,7,16] It is widely accepted that the charge separation mechanism at TiO_2/PbS QD interface behaves as a depleted p−n junction.[17,18] To maximize photon absorption and ensure that charge transport is electric field driven, it is essential to control the bulk morphology that phase separation between PbS and TiO_2 is at the same length of the depletion width within the PbS. Previous studies to create nanostructured TiO_2 templates used nanolithography[7,19] or liquid phase deposition techniques.[13,20] In this study we fabricate a porous TiO_2 template using polystyrene microspheres to create the optimum morphology for charge separation and transport.

RESULTS AND DISCUSSION

Using capacitance−voltage measurement, we determined the depletion width of our planar PbS/TiO_2 heterojunction at no applied bias to be 150 nm (Supporting Information) in agreement with another literature report.[17] However, the optical absorption at 900 nm in a 150 nm thick film is less than 30%,[6] and to achieve over 90% light absorption we would require a film thickness over 1 μm.[21] Hence, to increase the total absorber thickness, we need to create a macro-structured electrode. We postulate that the ideal porous structure for an all-inorganic bulk heterojunction which enhances charge extraction, while allowing for a thick active layer to maximize absorption, must have pore diameter on the length scale of twice the depletion width. This means that all photons are absorbed within the depletion region and charges generated at any point in the PbS-filled pores can be extracted by the internal electric field formed by the p−n junction. It is important that TiO_2 film is around 300 nm in order to create a monolayer of hollow spheres within the film. This ensures that all pores are open and can be infiltrated with PbS QDs and closed voids are predominantly avoided. An additional benefit

Received: June 5, 2014
Accepted: July 23, 2014
Published: July 23, 2014

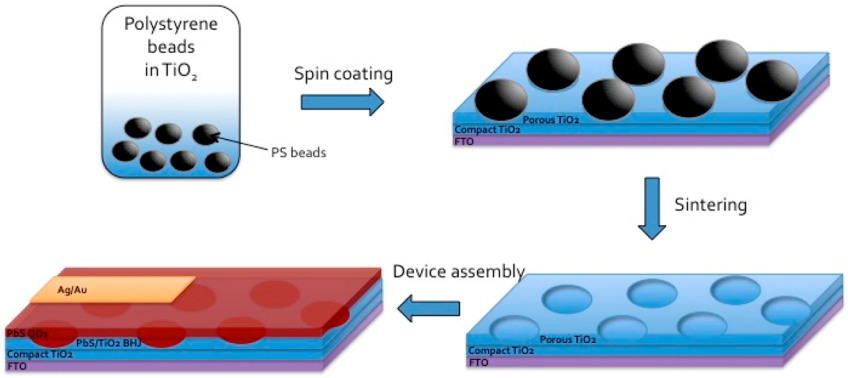

Figure 1. Schematic showing the preparation of macroporous TiO_2 templated PbS QD solar cell device.

of this structure is that light scattering is most effective in the visible to near IR region at these pore dimensions.

The fabrication process is summarized in Figure 1. On top of an FTO-coated glass substrate a compact layer of TiO_2 is deposited to avoid shunt paths forming between the PbS QDs and the FTO electrode. A composite film of TiO_2 containing 300 nm diameter polystyrene (PS) beads was then spin coated on top, followed by sintering in air at 500 °C. The sintering removes the organic binders from the TiO_2 and PS-beads, forming a porous TiO_2 film containing spherical voids mimicking the spherical shape of the PS sphere in the film. The hollow spheres were filled by spin coating PbS QDs from toluene solution, which allows the PbS to penetrate the pores. At the same time, a neat capping layer of PbS was built up on top, isolating the TiO_2 from the top electrode.

Scanning electron microscopy (SEM) images of the porous TiO_2 and a finished device are shown in Figure 2. A focused ion beam was used to prepare cross sections of the films. Images were taken using the backscattered detector and an accelerating voltage of 2 kV. This was chosen to maximize the contrast between the PbS and TiO_2. It can be seen that roughly 300 nm pores are created in a 300 nm TiO_2 thin film (Figure 2a). Some large pores can be seen on the surface, possibly due to agglomeration of the PS. Figure 2b shows the macro-pores were in-filled with PbS QDs with no voids observed. Figure 2c shows a reference planar junction device with well-defined interface between the PbS and TiO_2 layers.

In Figure 3 we show the $J-V$ characteristics of the highest efficiency macro-porous and planar junction devices. The best porous device produced a J_{sc} of 19 mA/cm^2, a V_{oc} of 0.51 V, a FF of 59% and a power conversion efficiency of 5.7%. The table compares the device parameters and standard deviations extracted from the current density-voltage ($J-V$) characteristic curves of all working devices. The devices with the porous structure exhibit an enhancement in short circuit current density under AM1.5G illumination. An enhancement in fill factor is also observed in the porous device, indicating reduced recombination. We find the series resistance is 4.7 Ω cm^2 for the macroporous device and 9.4 Ω cm^2 for planar this could result from the lowered dimensionality of the macroporous TiO_2 reducing charge scattering through the film and hence increasing the short circuit current we observe.

To understand the origin of the increased photocurrent in the porous TiO_2 structure, we looked for evidence from the enhancement of external quantum efficiency (EQE) at wavelengths from 400 to 1200 nm. The device with porous structure displays a higher EQE than the planar device across

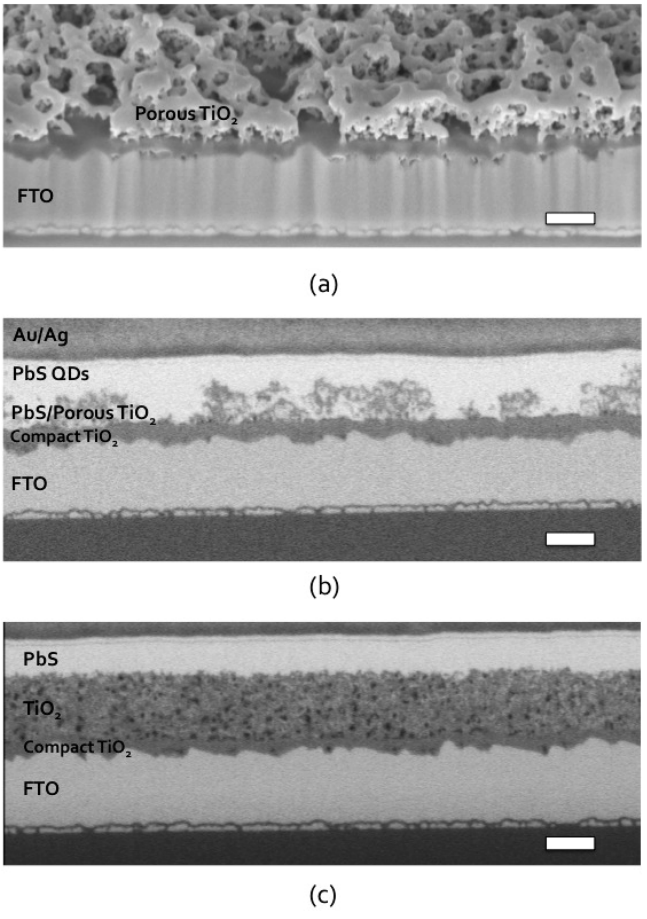

Figure 2. SEM images showing (a) the surface and cross-section image of the macroporous TiO_2 film on a FTO substrate. The pore dimension is consistent with the diameter of the polystyrene spheres used; (b) the electron backscattered images of the cross-section of a PbS/TiO_2 bulk heterojunction device and (c) a control planar junction device made under the same conditions. The scale bar is 300 nm in all image.

the whole range of wavelengths, particularly at short wavelengths. To elucidate the EQE enhancement, we first examine the optical properties of the devices.

In Figure 4 we show the absorption spectra of the planar and macroporous films. The measurement is performed with and without an integrating sphere. A significant increased absorption by the porous film is only observed below 700 nm. From the SEM cross-section images it is clear that there is

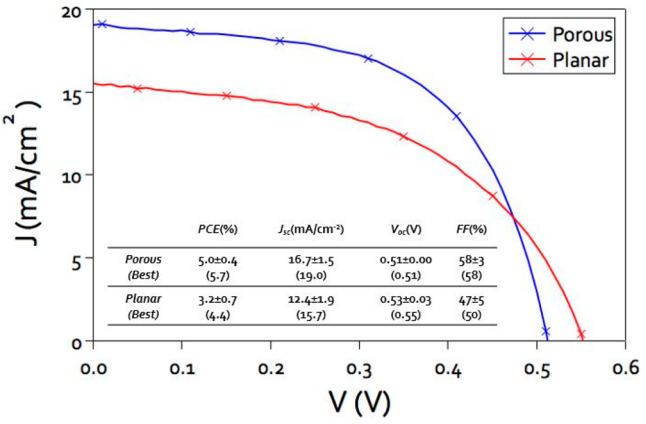

	PCE(%)	J_{sc}(mA/cm^2)	V_{oc}(V)	FF(%)
Porous (Best)	5.0±0.4 (5.7)	16.7±1.5 (19.0)	0.51±0.00 (0.51)	58±3 (58)
Planar (Best)	3.2±0.7 (4.4)	12.4±1.9 (15.7)	0.53±0.03 (0.55)	47±5 (50)

Figure 3. $J-V$ characteristic curves of the best porous and planar devices. The table lists the averaged device parameters for comparison.

roughly the same thickness of the neat PbS capping layers in both porous and planar devices, the difference being that the porous device has a higher overall volume of PbS as the QDs fill the pores. Furthermore, we can attribute some enhancement of photocurrent to increased absorption through light scattering within the porous structure. Yu et al.[22] suggest that a 300 nm pore size is most efficient in scattering light of visible wavelengths.[23] Our porous TiO_2 film looks visually translucent as the pores behave as scattering centers, leading to a better light management within the device. This scattering could explain the particular enhancement of absorption at the shorter wavelengths. The enhancement in EQE cannot be fully explained by the optical effects alone, as the porous film does not show higher optical absorption above 700 nm. Meanwhile, a higher fill factor suggests repressed recombination in this device and therefore we now proceed to examine the electronic properties.

Using semiconductor process simulation Kramer et al.[7] and Fan et al.[24] have shown an interpenetrated p−n junction device to be more efficient in charge extraction by suppressing Shockley-Read-Hall recombination. A significant increase in interface area means more carriers are generated in the vicinity of the junction interface, where the electric field strength is higher than the region further away from the junction. By this means the minority carrier rapidly drift to the interface for separation, reducing the occurrence of trap-assisted recombination. To measure whether the porous device can reduce trap-assisted recombination, small perturbation transient photocurrent decay measurements were performed on our devices.[20,25,26] These measurements allow us to monitor the fate of the excited carriers and to study the recombination and transport properties of the PbS/TiO_2 heterojunction devices. The cells are illuminated under simulated sunlight at different illumination intensities and "flashed" by a red light pulse generated by LEDs. The resulting transient photocurrent and photovoltage decays are then measured. The mean decay lifetime can be calculated by fitting the decay to an exponential function. The light pulse excites additional electrons which will decay with a lifetime τ.

The transient photocurrent decay curves of both devices measured at 1 sun background light intensity are shown in Figure 5a, the inset shows a close-up of the initial decay region. Both devices have rapid initial decays for 10 μs as free electrons drift out of the PbS to TiO_2 to produce current[27] as well as rapid trapping of the electrons.[28] However, the porous device shows a long-lived tail, with continuous charge extraction up to 3 ms. The origin of this long-lived photocurrent tail has been associated with a slow detrapping process[29] (Figure 5c). We note that both devices contain porous TiO_2, and that usually slow charge transport and detrapping is considered for transport within the TiO_2. However, the macro-porous PbS device here contains less TiO_2 than the planar film, and as such we expect the slow tail in the charge collection to be related to a mechanism in the PbS and not the TiO_2. This suggests that the BHJ has the ability to free charges from traps to produce higher photocurrent. In fact integrating the current decays for the two devices to obtain a collected charge, Q, the planar gives 5.65×10^{-9} C/cm^{-2} while the macroporous gives 4.88×10^{-8} C/cm^{-2}. The difference between these two, 4.31×10^{-8} C/cm^{-2}, is closely equal to the area under the slow component, indicating that this is precisely where the additional photocurrent is arising. This is probably assisted by the stronger electric field close to the interface of the BHJ such that trap-assisted recombination is reduced. To further verify whether this slow photocurrent decay dynamic is trap-meditated, we varied the background intensity as a means to change the charge occupation density of the trap states in the semiconductor. Figure 5b shows the transient photocurrent decay at different background light intensity. It is evident that a slower decay rate is observed with decreasing background intensity. At lower background intensity when more traps are unoccupied, there is a higher probability for electrons to be trapped in these

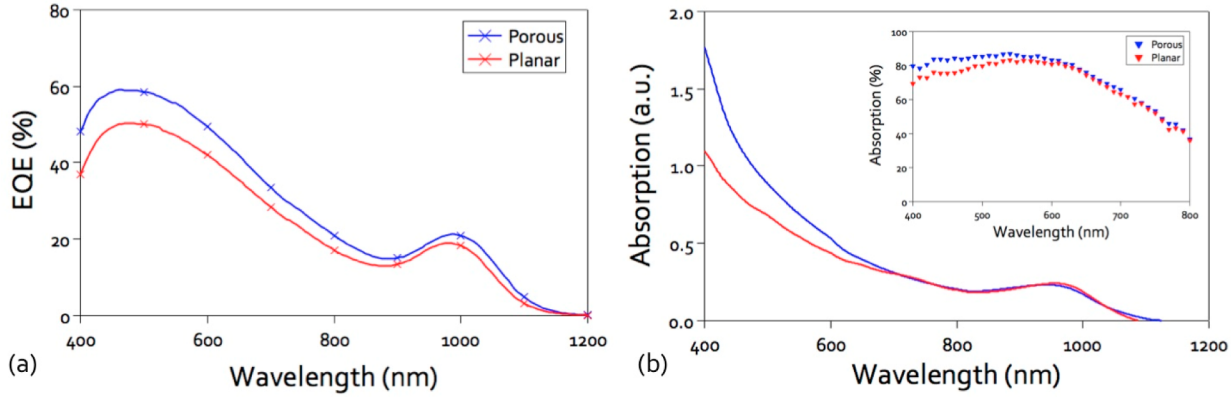

Figure 4. (a) External quantum efficiency of porous and planar devices from wavelength 400−1200 nm; (b) absorption spectra of planar and porous device film, inset showing the integrated sphere-corrected absorption spectra.

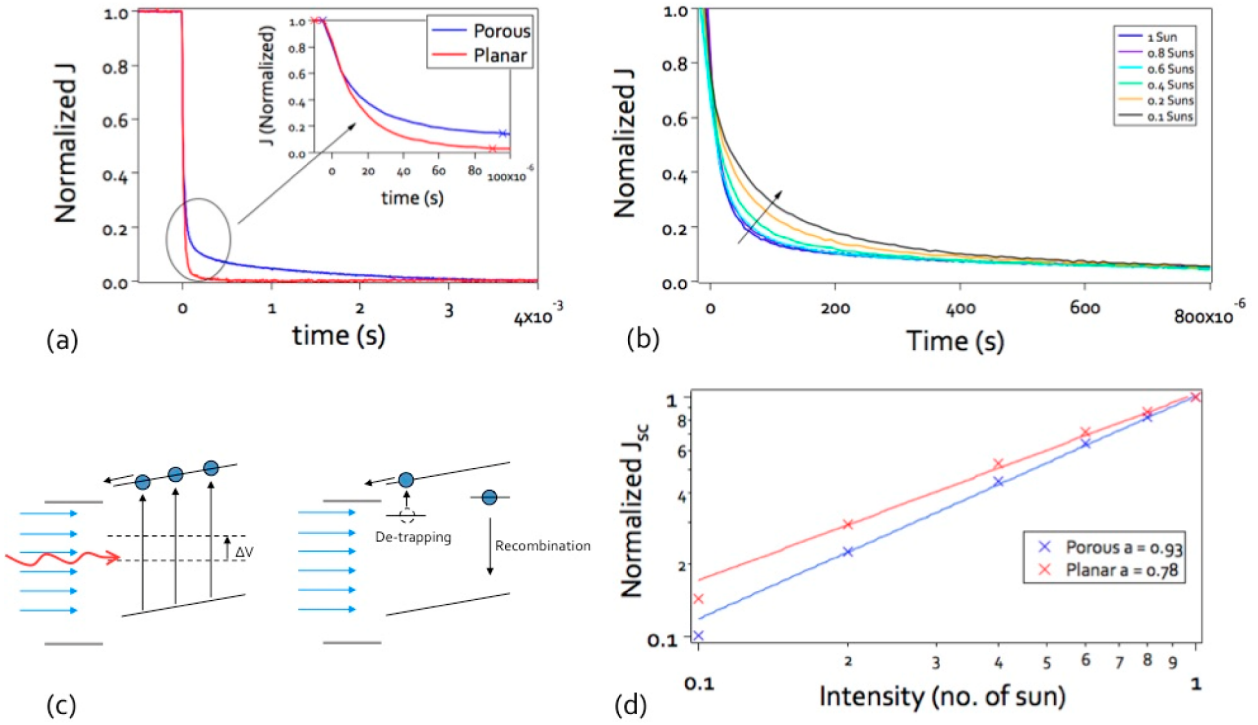

Figure 5. (a) Transient photocurrent decay of porous and planar junction devices at 1 sun background intensity; (b) transient photocurrent decay curves of a porous device at different background illumination intensity; (c) schematic illustrating the charge generation induced by the red-light pulse and the detrapping and recombination process in the depletion region. The detrapping process is likely to occur closer to the interface where a stronger electric field is present; (d) intensity-dependent measurement of normalized J_{sc}.

states. The calculated decay lifetime of the planar device is 24 μs, while the porous structure is 280 μs, suggesting terminal trapping of charges in the planar device, which subsequently recombine. The extended lifetime in the case of the porous structure suggests that the trapped charges can be subsequently extracted. This is confirmed by transient photovoltage decay measurements which are performed to directly measure the electron recombination lifetime under open-circuit conditions. Both planar and porous devices have the same recombination lifetime of around 20 μs when no charge extraction occurs. We note that under open-circuit, the charge density is much higher than under short-circuit conditions, and hence we expect faster charge recombination under open-circuit conditions. As such, the lifetime for recombination under open-circuit should not be quantitatively compared to the charge collection lifetime under short-circuit.

The light intensity dependence of the normalized J_{sc} is shown in Figure 5d. The data are fitted to the power law relationship,

$$J_{sc} \propto I^{\alpha} \quad (1)$$

The porous device produced a nearly linear relationship (α = 0.92) suggesting the device is operated with minimal bimolecular recombination, while a sublinear relationship is shown for the planar junction device with α = 0.78. Deviation of alpha to 1 is attributed to the formation of space charge[30] due to the unbalanced transport of electrons and holes, resulting in a significant increase in recombination.[31] The space charge effect is more significant in the planar device where the PbS layer thickness is much greater than the transport length of electrons.

CONCLUSION

In summary, improvement in the power conversion efficiency of QD solar cells has been demonstrated by using a template macroporous TiO_2. By using this bulk heterojunction structure, the short circuit current has been enhanced by over 30% compared with a planar junction device, along with a 10% increase in fill factor. The macroporous device allows a higher volume of PbS to absorb more photons while maintaining all charges to be extracted. Absorption has also been enhanced by the scattering effect of the porous structure, although at present this enhancement is of secondary importance. The BHJ structure also enhances the electronic properties by incorporating a large interface, showing a drastic increase in carrier lifetime for extraction.

EXPERIMENTAL SECTION

Details of the synthesis of PbS quantum dots and device fabrication are provided in the Supporting Information. SEM images were taken on a Zeiss NVision 40 FIB-SEM with a Schottky field emission Gemini column operated at 2 kV.

Macroporous TiO_2 electrodes are prepared as follows. Fluorine-doped tin oxide coated glass (Pilkington TEC 15) was rinsed with Milli-Q water, acetone, and ethanol and dried with clean dry air. The substrates were treated by oxygen plasma for 5 min. A compact layer of anatase TiO_2 was formed through spray pyrolysis of titanium diisopropoxide bis(acetylacetonate) diluted in anhydrous ethanol at a volumetric ratio of 1:10 using nitrogen as carrier gas. For a planar junction device, a TiO_2 layer was deposited by spin-coating TiO_2 paste (Dyesol 18NR-T) diluted in anhydrous ethanol at 1:4 by weight at 2000 rpm. For macroporous TiO_2 film, the same concentration of TiO_2 paste was mixed with polystyrene spheres. The layers were then sintered in air at 500 °C for 30 min.

Current−voltage characteristics were measured on a Keithley 2400 Sourcemeter under simulated AM 1.5G sunlight at 100 mW cm^{-2}

irradiance generated using an AAB ABET technologies Sun 2000 solar simulator and calibrated using an NREL calibrated silicon reference cell with a KG5 filter to minimize spectral mismatch (the mismatch factor was calculated to be less than 1%). The solar cells were masked with a metal aperture to define an active area of 0.09 cm^2 and measured in a light-tight sample holder to minimize any edge effects. To avoid overestimation of active area resulting in an erroneous short circuit current density,[32,33] metal apertures were applied to mask all our cells.

External quantum efficiency was measured by illuminating the devices by a halogen lamp fitted with an Oriel Cornerstone 130 monochromator. Light intensity at different wavelengths was calibrated using a Newport 818 UV enhanced silicon photodetector and a Newport 918 IR germanium photodetector. The current signal was measured with a Keithley 6845 picoammeter.

To measure the transient photocurrent and photovoltage decay, a white light bias was generated from an array of diodes (Lumiled model LXHL-NWE8 whitestar). The perturbation source was generated from a red-light pulsed diodes (LXHLND98 redstar, 200 μs square pulse width, 100 ns rise and fall time), controlled by a fast solid-state switch. The photovoltage decay was measured on a 1 GHz Agilent oscilloscope across the high impedance (1 MΩ) port, while the photocurrent decay was measured through a low impedance port (50 Ω) to enable short circuit condition.

■ ASSOCIATED CONTENT

Ⓢ Supporting Information

Details of PbS QD synthesis, preparation of porous TiO_2 template and device fabrication, capacitance−voltage data, and calculation of depletion width. This material is available free of charge via the Internet at http://pubs.acs.org.

■ AUTHOR INFORMATION

Corresponding Authors

*E-mail: h.snaith1@physics.ox.ac.uk.
*E-mail: andrew.watt@materials.ox.ac.uk.

Author Contributions

The manuscript was written through contributions of all authors. All authors have given approval to the final version of the manuscript. C.C. and M.M.L. contributed equally to the experimental aspects of this work.

Funding

We acknowledge funding from EPSRC (Platform Grant EP/F048009/1)

Notes

The authors declare no competing financial interest.

■ REFERENCES

(1) Tang, J.; Kemp, K. W.; Hoogland, S.; Jeong, K. S.; Liu, H.; Levina, L.; Furukawa, M.; Wang, X.; Debnath, R.; Cha, D.; Chou, K. W.; Fisher, A.; Amassian, A.; Asbury, J. B.; Sargent, E. H. Colloidal-Quantum-Dot Photovoltaics Using Atomic-Ligand Passivation. *Nat. Mater.* **2011**, *10*, 765−771.

(2) Ip, A. H.; Thon, S. M.; Hoogland, S.; Voznyy, O.; Zhitomirsky, D.; Debnath, R.; Levina, L.; Rollny, L. R.; Carey, G. H.; Fischer, A.; Kemp, K. W.; Kramer, I. J.; Ning, Z.; Labelle, A. J.; Chou, K. W.; Amassian, A.; Sargent, E. H. Hybrid Passivated Colloidal Quantum Dot Solids. *Nat. Nanotechnol.* **2012**, *7*, 577−582.

(3) Ning, Z.; Ren, Y.; Hoogland, S.; Voznyy, O.; Levina, L.; Stadler, P.; Lan, X.; Zhitomirsky, D.; Sargent, E. H. All-Inorganic Colloidal Quantum Dot Photovoltaics Employing Solution-Phase Halide Passivation. *Adv. Mater.* **2012**, *24*, 6295−6299.

(4) Zhitomirsky, D.; Furukawa, M.; Tang, J.; Stadler, P.; Hoogland, S.; Voznyy, O.; Liu, H.; Sargent, E. H. N-Type Colloidal-Quantum-Dot Solids for Photovoltaics. *Adv. Mater.* **2012**, *24*, 6181−6185.

(5) Liu, H.; Zhitomirsky, D.; Hoogland, S.; Tang, J.; Kramer, I. J.; Ning, Z.; Sargent, E. H. Systematic Optimization of Quantum Junction Colloidal Quantum Dot Solar Cells. *Appl. Phys. Lett.* **2012**, *101*, 151112.

(6) Barkhouse, D. A. R.; Debnath, R.; Kramer, I. J.; Zhitomirsky, D.; Pattantyus-Abraham, A. G.; Levina, L.; Etgar, L.; Grätzel, M.; Sargent, E. H. Depleted Bulk Heterojunction Colloidal Quantum Dot Photovoltaics. *Adv. Mater.* **2011**, *23*, 3134−3138.

(7) Kramer, I. J.; Zhitomirsky, D.; Bass, J. D.; Rice, P. M.; Topuria, T.; Krupp, L.; Thon, S. M.; Ip, A. H.; Debnath, R.; Kim, H.-C.; et al. Ordered Nanopillar Structured Electrodes for Depleted Bulk Heterojunction Colloidal Quantum Dot Solar Cells. *Adv. Mater.* **2012**, *24*, 2315−2319.

(8) Choi, J. J.; Wenger, W. N.; Hoffman, R. S.; Lim, Y.-F.; Luria, J.; Jasieniak, J.; Marohn, J. A.; Hanrath, T. Solution-Processed Nanocrystal Quantum Dot Tandem Solar Cells. *Adv. Mater.* **2011**, *23*, 3144−3148.

(9) Wang, X.; Koleilat, G. I.; Tang, J.; Liu, H.; Kramer, I. J.; Debnath, R.; Brzozowski, L.; Barkhouse, D. A. R.; Levina, L.; Hoogland, S.; Sargent, E. H. Tandem Colloidal Quantum Dot Solar Cells Employing a Graded Recombination Layer. *Nat. Photonics* **2011**, *5*, 480−484.

(10) Graetzel, M.; Janssen, R. a. J.; Mitzi, D. B.; Sargent, E. H. Materials Interface Engineering for Solution-Processed Photovoltaics. *Nature* **2012**, *488*, 304−312.

(11) Kramer, I. J.; Levina, L.; Debnath, R.; Zhitomirsky, D.; Sargent, E. H. Solar Cells Using Quantum Funnels. *Nano Lett.* **2011**, *11*, 3701−3706.

(12) Rath, A. K.; Bernechea, M.; Martinez, L.; Arquer, F. P. G.; De Osmond, J.; Konstantatos, G. Solution-Processed Inorganic Bulk Nano-Heterojunctions and Their Application to Solar Cells. *Nat. Photonics* **2012**, *6*, 529−534.

(13) Lan, X.; Bai, J.; Masala, S.; Thon, S. M.; Ren, Y.; Kramer, I. J.; Hoogland, S.; Simchi, A.; Koleilat, G. I.; Paz-Soldan, D.; Ning, Z.; Labelle, A. J.; Kim, J. Y.; Jabbour, G.; Sargent, E. H. Self-Assembled, Nanowire Network Electrodes for Depleted Bulk Heterojunction Solar Cells. *Adv. Mater.* **2013**, *25*, 1769−1773.

(14) Yu, G.; Gao, J.; Hummelen, J. C.; Wudl, F.; Heeger, A. J. Polymer Photovoltaic Cells: Enhanced Efficiencies via a Network of Internal Donor-Acceptor Heterojunctions. *Science* **1995**, *270*, 1789−1791.

(15) Cho, S.; Coates, N.; Moon, J. S.; Park, S. H.; Roy, A.; Beaupre, S.; Moses, D.; Leclerc, M.; Lee, K.; Heeger, A. J. Bulk Heterojunction Solar Cells with Internal Quantum Efficiency Approaching 100%. *Nat. Photonics* **2009**, *3*, 297−303.

(16) Willis, S. M.; Cheng, C.; Assender, H. E.; Watt, A. A. R. The Transitional Heterojunction Behavior of PbS/ZnO Colloidal Quantum Dot Solar Cells. *Nano Lett.* **2012**, *12*, 1522−1526.

(17) Pattantyus-Abraham, A. G.; Kramer, I. J.; Barkhouse, A. R.; Wang, X.; Konstantatos, G.; Debnath, R.; Levina, L.; Raabe, I.; Nazeeruddin, M. K.; Grätzel, M.; Sargent, E. H. Depleted-Heterojunction Colloidal Quantum Dot Solar Cells. *ACS Nano* **2010**, *4*, 3374−3380.

(18) Etgar, L.; Moehl, T.; Gabriel, S.; Hickey, S. G.; Eychmüller, A.; Grätzel, M. Light Energy Conversion by Mesoscopic PbS Quantum dots/TiO_2 Heterojunction Heterojunction Solar Cells. *ACS Nano* **2012**, 3092−3099.

(19) Kim, S.; Kim, J. K.; Gao, J.; Song, J. H.; An, H. J.; You, T.; Lee, T.; Jeong, J.; Lee, E.; Jeong, J.; Beard, M. C.; Jeong, S. Lead Sulfide Nanocrystal Quantum Dot Solar Cells with Trenched ZnO Fabricated via Nanoimprinting. *ACS Appl. Mater. Interfaces* **2013**, *5*, 3803−3808.

(20) Leschkies, K. S.; Jacobs, A. G.; Norris, D. J.; Aydil, E. S. Nanowire-Quantum-Dot Solar Cells and the Influence of Nanowire Length on the Charge Collection Efficiency. *Appl. Phys. Lett.* **2009**, *95*, 193103.

(21) Wu, H.; Yang, Y.; Oh, E.; Lai, F.; Yu, D. Direct Synthesis of High-Density Lead Sulfide Nanowires on Metal Thin Films Towards Efficient Infrared Light Conversion. *Nanotechnology* **2012**, *23*, 265602.

(22) Yu, I. G.; Kim, Y. J.; Kim, H. J.; Lee, C.; Lee, W. I. Size-Dependent Light-Scattering Effects of Nanoporous TiO2 Spheres in Dye-Sensitized Solar Cells. *J. Mater. Chem.* **2011**, *21*, 532−538.
(23) Ferber, J.; Luther, J. Computer Simulations of Light Scattering and Absorption in Dye-Sensitized Solar Cells. *Sol. Energy Mater. Sol. Cells* **1998**, *54*, 265−275.
(24) Fan, Z.; Razavi, H.; Do, J.; Moriwaki, A.; Ergen, O.; Chueh, Y.-L.; Leu, P. W.; Ho, J. C.; Takahashi, T.; Reichertz, L. A.; Neale, S.; Yu, L.; Wu, M.; Ager, J. W.; Javey, A. Three-Dimensional Nanopillar-Array Photovoltaics on Low-Cost and Flexible Substrates. *Nat. Mater.* **2009**, *8*, 648−653.
(25) Snaith, H. J.; Moule, A. J.; Klein, C.; Meerholz, K.; Friend, R. H.; Grätzel, M. Efficiency Enhancements in Solid-State Hybrid Solar Cells via Reduced Charge Recombination and Increased Light Capture. *Nano Lett.* **2007**, *7*, 3372−3376.
(26) O'Regan, B. C.; Lenzmann, F. Charge Transport and Recombination in a Nanoscale Interpenetrating Network of n-Type and p-Type Semiconductors: Transient Photocurrent and Photovoltage Studies of TiO_2/Dye/CuSCN Photovoltaic Cells. *J. Phys. Chem. B* **2004**, *108*, 4342−4350.
(27) Lee, M. M.; Teuscher, J.; Miyasaka, T.; Murakami, T. N.; Snaith, H. J. Efficient Hybrid Solar Cells Based on Meso-Superstructured Organometal Halide Perovskites. *Science* **2012**, *338*, 643−647.
(28) Li, Z.; McNeill, C. R. Transient Photocurrent Measurements of PCDTBT:PC70BM and PCPDTBT:PC70BM Solar Cells: Evidence for Charge Trapping in Efficient Polymer/fullerene Blends. *J. Appl. Phys.* **2011**, *109*, 074513.
(29) McNeill, C. R.; Hwang, I.; Greenham, N. C. Photocurrent Transients in All-Polymer Solar Cells: Trapping and Detrapping Effects. *J. Appl. Phys.* **2009**, *106*, 024507.
(30) Koster, L. J. A.; Mihailetchi, V. D.; Xie, H.; Blom, P. W. M. Origin of the Light Intensity Dependence of the Short-Circuit Current of Polymer/Fullerene Solar Cells. *Appl. Phys. Lett.* **2005**, *87*, 203502.
(31) Mihailetchi, V. D.; Wildeman, J.; Blom, P. W. M. Space-Charge Limited Photocurrent. *Phys. Rev. Lett.* **2005**, *94*, 126602.
(32) Snaith, H. J. How Should You Measure Your Excitonic Solar Cells? *Energy Environ. Sci.* **2012**, *5*, 6513−6520.
(33) Snaith, H. J. The Perils of Solar Cell Efficiency Measurements. *Nat. Photonics* **2012**, *6*, 337−340.